

The Development of Ion Nano-beams - A Review

S. Kalbitzer

Ion Beam Technology, Amselgasse 11, Heidelberg 69121, Germany

V."A."Zhukov

St Petersburg Institute for Informatics and Automation, St Petersburg 199178, Russia

Received: November 7, 2011

Accepted: December 1, 2011

Published: February 1, 2012

doi:10.5539/apr.v4n1p211

URL: <http://dx.doi.org/10.5539/apr.v4n1p211>

Abstract

With the advent of the super-tip ion source very favourable conditions for generating ion nano-beams have been provided. The basic physical principles for a super-tip-gas field ion source are described. As a consequence of a very small source emittance of $\epsilon \sim 10^{-24} \text{ m}^2\text{sr}$ ultra-bright rare gas ion beams of about $10^{16} \text{ A/m}^2\text{.sr}$ can be produced. As a further consequence, very narrow probe sizes are obtainable, of $d_p < 1 \text{ nm}$, with spatial resolutions far below the classical limits of light-optics and even below the novel stimulated-emission-depletion microscopy [*STED (microscopy) = stimulated emission depletion (microscopy) Th. A. Klar, S. W. Hell, Opt.Lett. 24 (1999) 954-956]. Various ion-nanobeam applications in both materials modification, and analysis are envisaged.

Keywords: Ion nano beam, Gas field ion source

1. Introduction

The fundamental question of how to generate ion nano-beams is intimately connected with the ionisation mechanism of the source operated with gaseous media.

The decisive figure of merit is beam emittance, which controls the properties of the image spot, e.g. the diameter of the beam probe. If nanometre dimensions are intended, almost all presently known ion source types can be excluded because of very unfavourable emittance figures. So far, only by using very narrow apertures, with concomitant high losses of intensity, fine ion beams have been obtained, as often practised in PIXE applications. Thus, the only remaining option is the development of the Müller field-ion microscope, with proven atomic resolution, to an efficient gas field ion source. It is the aim of this paper to follow this development over a period of more than 10 years.

2. Base Tip Preparation

The central element of a gas field ion source, GFIS, usually is a 111-monocrystalline tungsten wire of a few tenths mm in diameter with an acute tip. The starting base tip can be produced by anodic dissolution of W in a solution of NaOH within a few minutes of exposure to dc or pulsed-current treatments. Tip radii of 100-1000 nm are readily obtaind by electrolytic etching. (S. Pinter, 1985)

3. Formation of the Super-tip

The experimental set-up is shown in fig1. (K. Jousten, K. Böhringer, & S. Kalbitzer, 1988). It provides both cooling to low cryogenic temperatures and heating to about 2500 K. Also high voltages of $U \sim 50 \text{ kV}$ can be applied. While Müller's ion-field microscope is useful for exploration of atomic surfaces with atomic resolution, the emitted ion beam, however, comes from a large number of emission sites distributed over the apex zone. With a regular W-tip He^+ emission occurs over a broad angular range of $\alpha/2 \sim 50^\circ$.

For use as an ion source, however, both emission angle and number of emitting sites have to be strongly reduced in order to provide a high-brightness beam and also an intense ion probe. The experimental task, therefore, has been to produce a single emitter point with a small virtual source size as illustrated by fig.2. This goal can be achieved by a relatively complex procedure to form the so-called super-tip. (K. Jousten, K. Böhringer, & S. Kalbitzer, 1988). First experimental attempts along these lines, however, did not result in long-term stable protrusions.(P. R. Schwoebel, & G.R. Hanson, 1985) In a short description, the etched tip has first to be cleaned from any adhering impurity layer by heating to about 2500 K for a few minutes. Thereafter, the tip is operated in

the electron emission mode in a He atmosphere of about 0.1 Pa. He ions generated by electron impact are accelerated back to the tip, where W surface atoms, created by impact of He^+ , diffuse at temperatures of $T \sim 1000$ K to preferred crystallographic surface sites. Within one minute's time they self-organise into a nano-crystalline structure, constituting the super-tip. While single W adatoms, lacking bulk binding forces, constitute less stable configurations against thermal and electrical attack, the crystalline structure of our super-tip offers enhanced stability against all desorption processes. Because of the rapid increase of the electron emission during super-tip formation, as fig.5 demonstrates, a fast switch-off of the bias volt has to be performed in order to prevent thermal self-destruction of the growing super-tip. (R. Börret, 1989)

A single emission centre of a super-tip was displayed on the phosphorescent screen of fig.1. (K. Jousten, 1987) The spot diameter was 1.1mm at a distance of 0.07m, so that the emission half-angle amounts to $\alpha/2 \sim 0.55 \cdot 10^{-3}$ /0.07~ 0.08.mrad. Thus, the goals of fig.4 appear feasible. An ion-field micrograph of this super-tip with He as imaging gas is shown in fig.4, displaying a W. nano-crystallite of about 100 W-surface-atoms on top of the initial apex of the base tip. (Th. Miller, 1996). This is established by all experimental observations with our multi-atom super-tip for all rare gas elements. Fig 5 is a statistical survey over about 40 super-tip formation sites placed within an average angular range of about 10° off the center direction of 111-tips.(Th. Miller, A. Knoblauch, & S. Kalbitzer, 1997)

3.1 Current-field Characteristics of GFIS Sources

The thermal gas supply to the emitter shank is given by the relation

$$J_0 = n_0 \sigma(\Phi) A v \quad (1)$$

where the atomic velocity v is given by

$$v = (2kT/m)^{1/2} \quad (2)$$

The flux enhancement factor $\sigma(\Phi)$ contains the variable $\Phi = \frac{1}{2}\alpha F^2/kT$, the ratio of the gas polarisation energy $\frac{1}{2}\alpha F^2$ and the thermal energy kT . Φ is the most important parameter for a gas field ion source controlling both gas supply to and an efficient transport along the tip surface to the emitting apex. As suggested by fig.9 the exposed emitter area of a hemispherical tip-surface, with a diameter of $d \sim 300$ nm, is estimated as $A \sim \frac{1}{4}\pi d^2 \sim 8 \cdot 10^{-14} \text{ m}^2$, respectively. Using the approximation for a paraboloidal emitter tip (H. A. M, van Eekelen, 1970):

$$\sigma(\Phi) = \frac{1}{4} (\Phi + 2.7\Phi^{2/3} + 2.7\Phi^{1/3} + 1), \quad (3)$$

we note that $\sigma(\Phi)$ substantially enhances the gas flow to the emitter area. For $\sigma(0)$ and a gas pressure of 0:1 Pa J_0 amounts to roughly $3 \cdot 10^{19}$ at/s.m², and with $v \sim 10^3$ m/s and $\Phi \sim 20$ we have $j(\Phi) \sim 6 \cdot 10^{23}$ at/m².s. Thus, the total gas flow to a tip area of about 10^{-13} m^2 amounts to about $6 \cdot 10^{10}$ at/s.or roughly to an electrically equivalent ion current of 10 nA for a fictitious 100% ionisation yield. Figs.6 and 7 confirm the linear dependence on gas pressure in (1) with very strong emission currents of up to $j(\text{H}_2^+) \sim 100$ nA at 0.1 Pa. Table 1 provides a survey over some basic rare gas properties. In agreement with experimental data, we see that the supply gas flow (1) approximately depends on the quantity $\rho \sim \alpha^{2/3}/m^{1/2} \sim 0.2 \text{ \AA}^2/\text{amu}^{1/2}$ for all heavier rare gases at same source operation conditions. Thus, we very roughly expect similar current-field characteristics for all of them. In general, the very steep rise of $j(F)$ observed at the lower electrical fields levels off at higher fields. Explanations invoking temperature independent tunnelling processes, however, have to be replaced by loss of adsorbed gas atoms from the surface with an activated exponential temperature dependence, as will be shown below. In the flat region of supply limited current a linear dependence on gas pressure exists as shown in fig 11. Fig.8 shows two typical I(V) characteristics of H_2^+ at different gas temperatures of 90K and 270K. We note that $\sigma(\Phi)$ can explain the observed current differences. (H. A. M, van Eekelen, 1970) It is interesting to see from fig.9 that tip geometry has a strong influence on the emitted current intensity: $I \propto r_t^2$, indicating spherical supply areas. (R. Börret, 1989)

3.2 Energy distribution of extracted ion beams

Using a retarding potential technique we have measured the chromatic widths of our nano-beams.(Th. Maisch, et al., 1991) In general, we found for all ion species values of $\Delta E \leq 1$ eV (FWHM) or $\sigma \leq 0.4$ eV, co-determining chromatic aberration. Fig.10 presents the case of He^+ , fig.11 of Ne^+ . Also, for H_2^+ $\Delta E \sim 1$ eV(FWHM) applies. It appears that ion mass influences these figures. We speculate that thermal velocities/vibrations $\propto m^{-1/2}$ are involved. $\Delta E(\text{H}_2^+)/\Delta E(\text{He}^+)/\Delta E(\text{Ne})$ as indicated by experimental figures of $\Delta E \sim 1/0.7/0.5$.

3.3 Beam emittance and brightness of super-tips

With the above value of $\alpha/2 \sim 8$ mrad and a calculated virtual source size of $d \sim 1\text{\AA}$, the emittance amounts to $10^{-24} \text{ m}^2 \text{sr}$ (S. Kalbitzer & A. Knoblauch, 2004) which is the most important parameter for the design of a low aberration ion optical column. Assuming probe currents of up to 10 nA the correlated brightness amounts to $B = I/\epsilon < 10^{16} \text{ A/m}^2 \text{sr}$, hitherto unparalleled by any other particle source, as shown in fig.12.

3.4 Optical consequences

A tip surface of a hemi-sphere of $A \sim 1.10^{-13} \text{ m}^2$ captures about 3.10^{11} atoms/s. Fig.13 displays probe diameters and correlated current intensities as a function of the probe convergence angle. (S. Kalbitzer & V A. Zhukov, 2011).

The above figures are very consequential for ion probe dimensions.

A general estimate of limiting probe spot radii $r_p = d_p/2$ reads (G. F. J. Legge, 1987):

$$r_p^2 = r_s^2 + r_c^2 + r_d^2,$$

with probe diameters of $d_s = \frac{1}{2} C_s \alpha_p^3$ $d_c = 2\eta C_c \alpha_p$ $d_d = 2\eta C_d \alpha_p^{-1}$

with a minimum of $r_{min} = 0.773(C_c\eta)^{1/2}(\Lambda^2 + 2.687r_0^2\alpha_0^2\eta)^{1/4}$, where r_0 and α_0 are the key constituents of the correlated source emittance ϵ . Fig. 13 is a plot of probe size d_p and correlated probe current I_p vs. convergence angle α_p . (S. Kalbitzer, 2004)

Employing the emittance variable ϵ for the limiting cases of purely chromatic and spherical aberrations $d \approx d_c = 2C_c^{1/2}\eta^{1/2}\epsilon^{1/4}$, $d = d_s \approx 2C_s^{1/4}\epsilon^{3/8}$, (T. Butz & G. J. F. Legge, 1996) we clearly see that a major reduction of source emittance is absolutely necessary to a sizeable improvement of former probe spots of $d_p \sim 30$ nm to presently $d_p \sim 1$ nm.

We note that the tip geometry enters eq(3). as the target area of the incoming gas flux. In particular, experimental findings show a dependence on the tip radius by r_t as shown above by fig.9. (R. Börret, 1989) For conservative values of the aberration coefficients $C_c = 0.1$ m and $C_s = 1$ m we find with $\eta \sim 10^{-5}$ limiting values of $d_c \sim 2$ nm and $d_s \sim 2$ nm, i.e. resolutions in the atomic regime. Thus, a GFIS* promises intense Xenon beam-probes of nano-metre dimensions.

There is some uncertainty about the diffusion behaviour of Xe on W surfaces.(R. Gomer, 1961) While Kr and Ar exhibit relatively low diffusion activation energies of $Q_D \sim 40 - 30$ meV, $Q(Xe) \sim 130$ meV is distinctly higher.(R. Gomer,1961). Nevertheless, as fig. 14 shows, even for Q_D values of 80, 100 and 130 meV probe currents of $j(Xe) \sim 5$ nA are possible with appropriately chosen super-tip temperatures and fields.

According to a thermodynamic formulation, the GFIS* emitter current can be written (see chapter 4) (S. Kalbitzer, 2004):

4. Thermodynamic theory of a GFIS*-source

The emitter current is given by the integral over several physical processes:

$$J(z, F, kT) = j_0 \int \sigma \theta \eta \zeta dA(z) dz, \quad (4)$$

where z is the distance from the emitter apex, $A(z)$ the tip surface elemental area, F the electrical field strength, T the tip temperature, j_0 the gas kinetic supply from the gas phase, σ the field enhancement factor of gas supply, θ the Langmuir equilibrium state of occupied surface states, η the transport efficiency of adsorbed atoms and ζ the ionisation probability at the super-tip. Ion source properties: Current: $I < 10^{-8}$ A, source emittance: $10^{-24} \text{ m}^2 \text{ sr}$, source brightness: $B = I/\epsilon < 10^{16} \text{ A/m}^2 \text{ sr}$.

Fig.12 presents a comparison of different types of ion sources and emphasizes the unique properties of our GFIS*.

$A(z)$ is the tip surface elemental area. A detailed description of the functions in the above integral was published elsewhere.(S. Kalbitzer, 2004). Here we just emphasize that the predicted steep slopes of $dI/dF = m$ range up to $m= 60$ in the low field emission regime compatible with experimental observations. Also, emitter currents of the system Ar-W with a paraboloidal emitter shape are correctly predicted as of the order of $I \sim 10$ nA in the supply limited regime. In conclusion, we maintain that eq.(3) is a valid description of the GFIS* emitter current. strength. (S. Kalbitzer, 2004; Th. Maisch, et al., 1991; S. Kalbitzer & A. Knoblauch, 2004; S. Kalbitzer & V A. Zhukov, 2011)

5. Applications of rare gas nano-beams to materials research

As previously described (S. Kalbitzer & V A. Zhukov, 2011) in some detail, using rare gases one can perform machining, deposition, amorphisation, TOF-SIMS (A. Benninghoven, B. Hagenhoff, & E. Niehuis, 1993) ,

permanent data storage and high resolution surface imaging in the nano-regime. (B. W. Ward, J. A. Notte, & N. P. Economou, 2006).

In final conclusion, rare gas ion nano-beams constitute a unique tool for materials nano-research and technology.

References

- A. Benninghoven, B. Hagenhoff, & E. Niehuis. (1993). Surface MS – Probing Real World Samples. *Analytical Chemistry*, 65, 630A-640A. <http://dx.doi.org/10.1021/ac00062a002>
- B. W. Ward, J. A. Notte, & N. P. Economou. (2006). Helium ion microscope: A new tool for nanoscale microscopy and metrology. *J. Vac. Sci. Technol. B*, 24(6), 2871-74. <http://dx.doi.org/10.1116/1.2357967>
- G. F. J. Legge. (1987). The Limits of Spatial Resolution in PIXE. *Nucl. Instr. and Meth. B*22, 115-120.
- H. A. M. van Eekelen. (1970). The behaviour of the field-ion microscope: A gas dynamical calculation. *Surface Science* 21, 21. [http://dx.doi.org/10.1016/0039-6028\(70\)90061-0](http://dx.doi.org/10.1016/0039-6028(70)90061-0)
- K. Jousten, K. Böhringer, & S. Kalbitzer. (1988). Current-Voltage Characteristics of a Gas Field Ion Source. *Appl. Phys., B46*, 313-323. <http://dx.doi.org/10.1007/BF00686454>
- K. Jousten. (1987). Der Aufbau einer Gasfeldionisationsquelle. Doctoral dissertation, University of Heidelberg.
- P. R. Schwoebel, & G.R. Hanson. (1985). Beam current stability from localized emission sites in a field ion source. *J. Vac. Sci. Technol., B3*, 214-219.
- R. Börret. (1989). Herstellung und Eigenschaften strukturierter Feldemitter für Ionenmikrostrahlen. Doctoral dissertation, University of Heidelberg.
- R. Gomer. (1961). Field Emission and Field Ionization. *Harvard University Press*, Cambridge, Massachusetts, 134-136
- S. Kalbitzer, & A. Knoblauch. (2004). Physical processes in a super-tip gas field ion source. *Appl. Phys., A78*, 269-281. <http://dx.doi.org/10.1007/s00339-003-2218-1>
- S. Kalbitzer, & V A. Zhukov. (2011). Xenon nano-beams for materials research. *Radiation Effects & Defects in Solids iFirst*, 1-10.
- S. Kalbitzer. (2004). Optimised operation of gas field ion source. *Appl. Phys. A79*, 1901-1905. <http://dx.doi.org/10.1007/s00339-004-2869-6>
- S. Pinter. (1985). Diploma work at the Max-Planck-Institut für Kernphysik:Herstellung und Eigenschaften von Wolfram-Feldemissionsspitzen.
- T. Butz, & G. J. F. Legge. (1996). From micro- to nanoprobe: auspices and horizons. *Nucl. Instrum. and Methods, B113*, 317- 322.
- T. T. Tsong. (1990). *Atom-probe Field Ion Microscopy*. Cambridge University Press, 167
- Th. Maisch, Ch. Wilbertz, Th. Miller, & S. Kalbitzer. (1991). Energy spread of a focused ion beam system with a super-tip. *Nucl.Instr.,and Meth. B80/81*, 1288-1291.
- Th. Miller, A. Knoblauch, & S. Kalbitzer. (1997). Atomic Structure and Electrical Properties of a Super-tip Gas Field-Ion Source. *Materials Forum, Vols. 248-249*, 433-438.
- Th. Miller, A. Knoblauch, Ch. Wilbertz, & S. Kalbitzer. (1995). Field-ion- imaging of a tungsten super-tip. *App. Phys., A61*, 99-100.
- Th. Miller. (1996). Atomarer Aufbau und elektrische Eigenschaften nanostrukturierter Feldionisationsquellen. Doctoral dissertation, University of Heidelberg.

Table 1. Rare gas properties

Gas	Z/M	Tc (K)	$\alpha(A^3)$	X(eV)	v(cm/s)	$\Lambda(fm)$	Y(W)	S	I(nA)	$\alpha^{2/3}/m^{1/2}$
He	2/4	4.2	0.20	24.5	9×10^5	143	~5	<0.2 ¹	2	0.17
Ne	10/20	27.1	0.39	21.5	4×10^5	64	<4*	<0.8	2	0.12
Ar	18/40	87.3	1.62	15.7	2.8×10^5	45	<3*	<3	2	0.22
Kr	36/84	120.1	2.47	13.9	2.0×10^5	31	<2*	<2	2	0.20
Xe	54/131	165.9	4.06	12.1	1×10^5	25	<1	<10	2 ^{&}	0.22

$\rho = \alpha^{2/3}/m^{1/2}$, & extrapolated value,¹ at E ~1keV , * estimated by the relation ionisation energy/tungsten work function Y~X/W-1, W(W)~ 4.5 eV

Notes: T_c , gas condensation temperature; α , polarisability; X , ionisation potential, v ion velocity; Λ , de Broglie wavelength; I , emitter currents at $p \sim 0.1$ Pa; Y (electrons/ion), secondary electron yield; S (atoms/ion), sputtering yield; ion energy $E \sim 10$ keV.

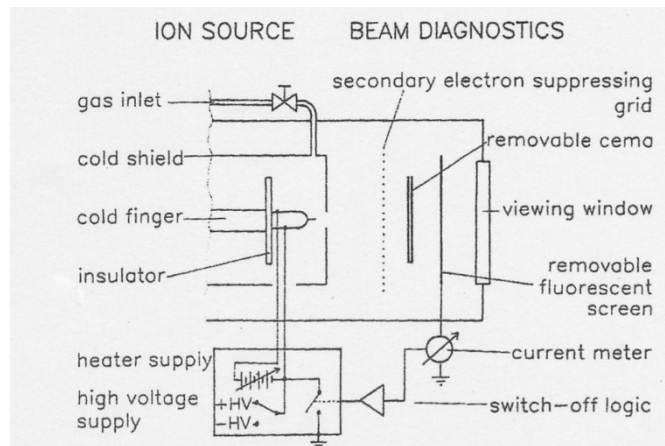


Figure 1. Experimental set-up for super-tip production

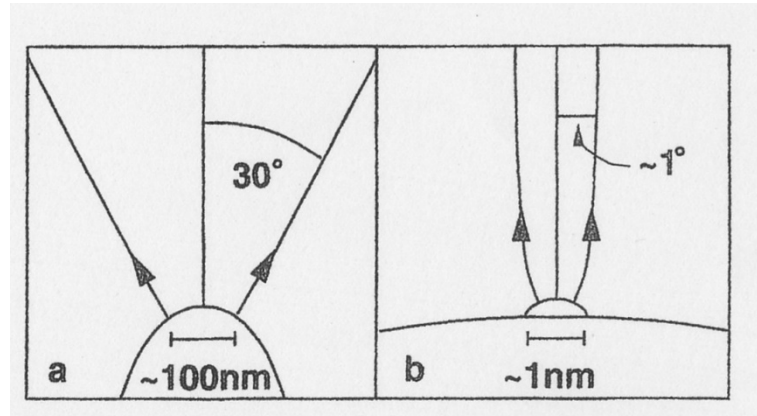


Figure 2. Scheme of the emission geometry of a regular tip (a) and an intended super-tip on top of a regular tip (b)

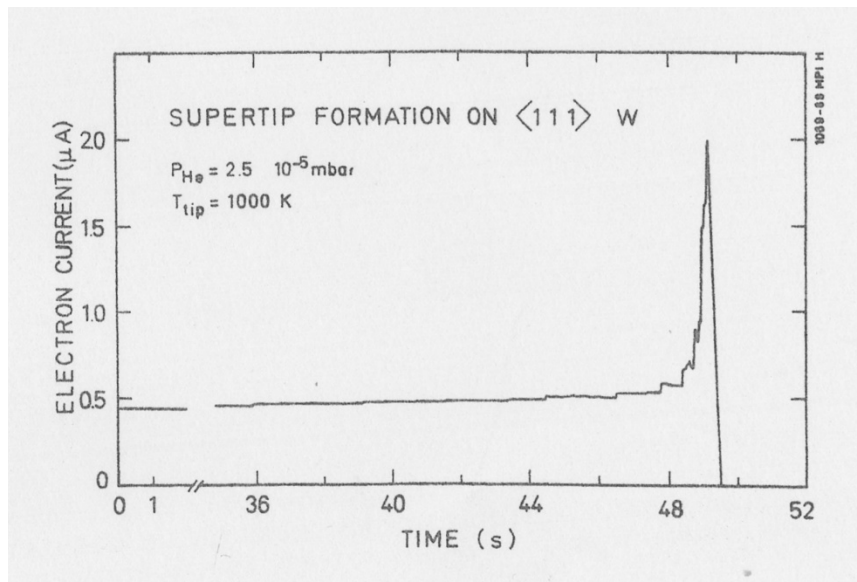


Figure 3. Electron emission current during super-tip formation on a 111-W tip

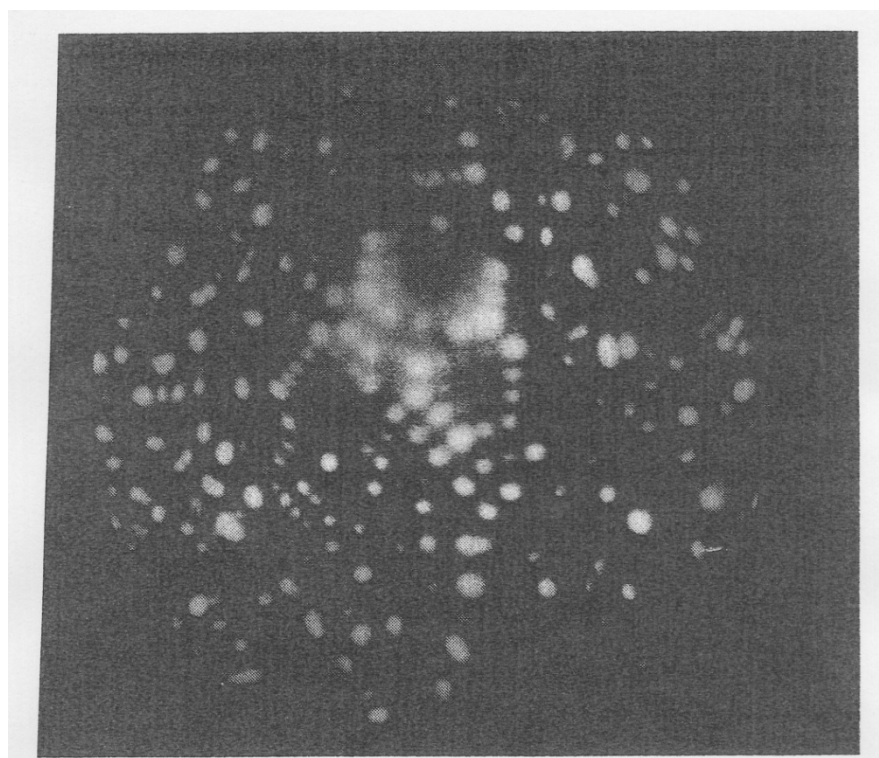


Figure 4. Field-ion micrograph of the super-tip with He as imaging gas. This nano-crystalline structure contains a total of about 100 W atoms. Its physical extension is about $\pm 2\text{nm}$, or 5W atoms on each side

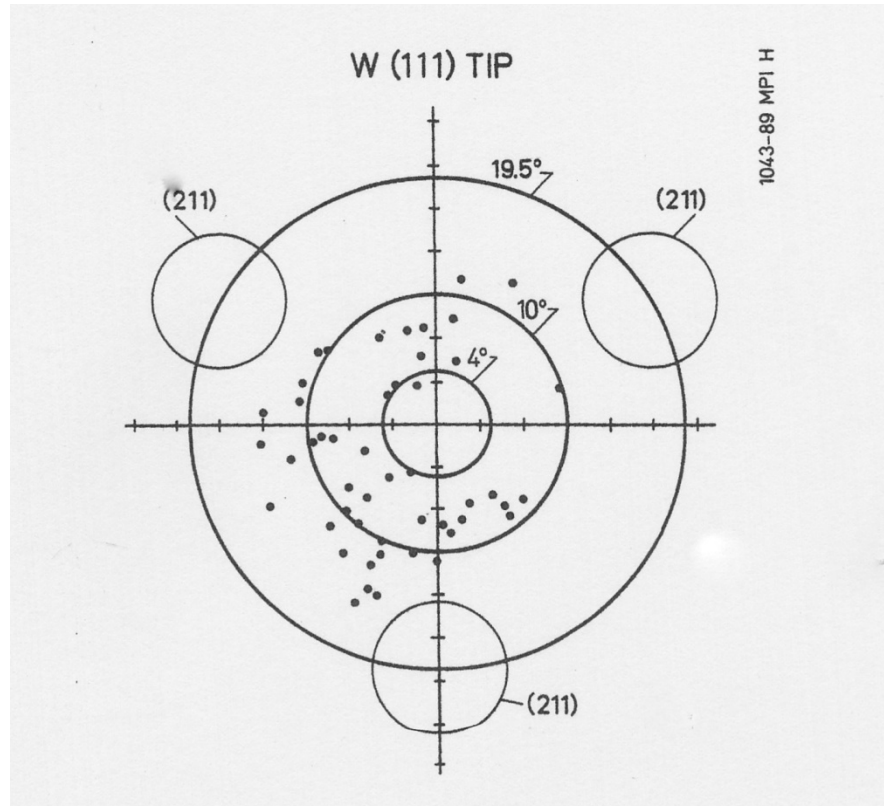


Figure 5. Distribution of super-tip locations on the 111-W tip-surface

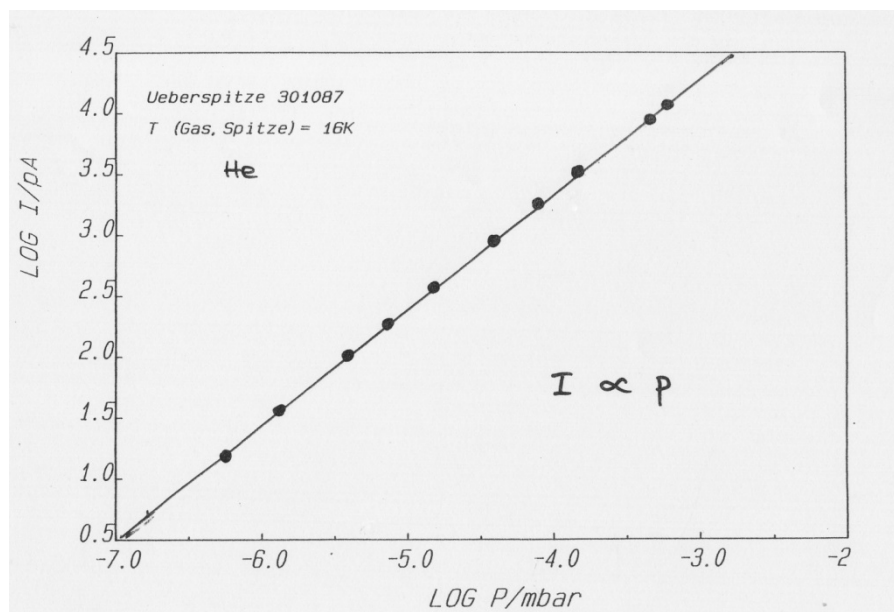


Figure 6. Ion emission current $I(\text{He}^+)$ as a function of He gas pressure. $I(0.1 \text{ Pa}) \sim 10 \text{ nA}$

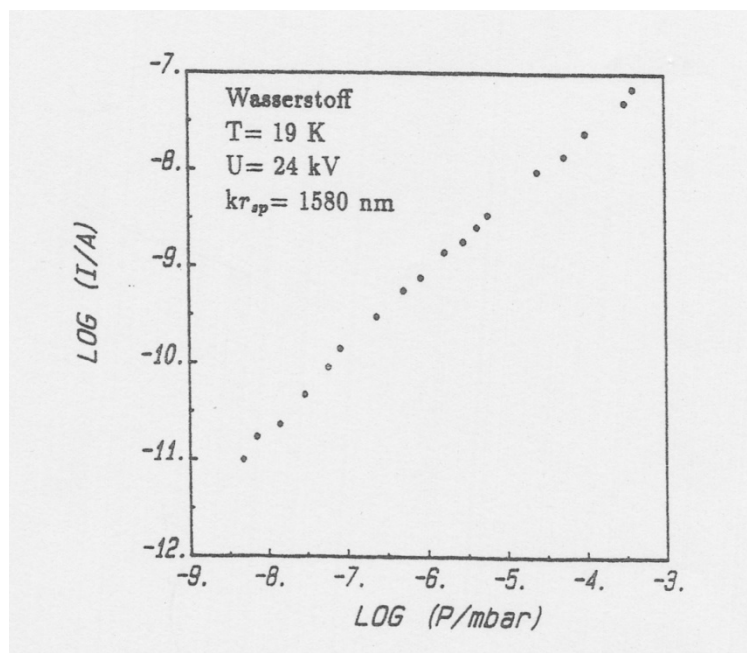


Figure 7. Ion emission current $I(\text{H}_2^+)$ as a function of H_2 gas pressure $I(0.1 \text{ Pa}) \sim 100 \text{ nA}$

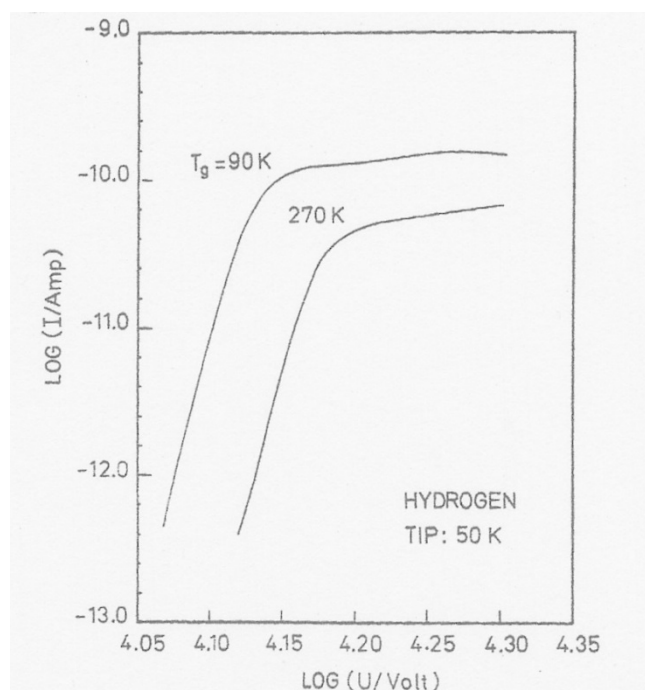
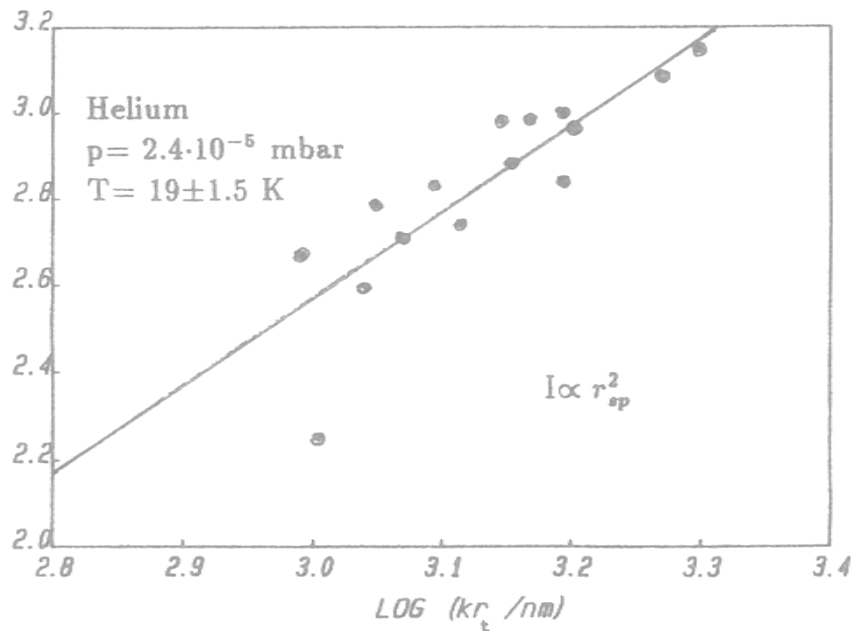
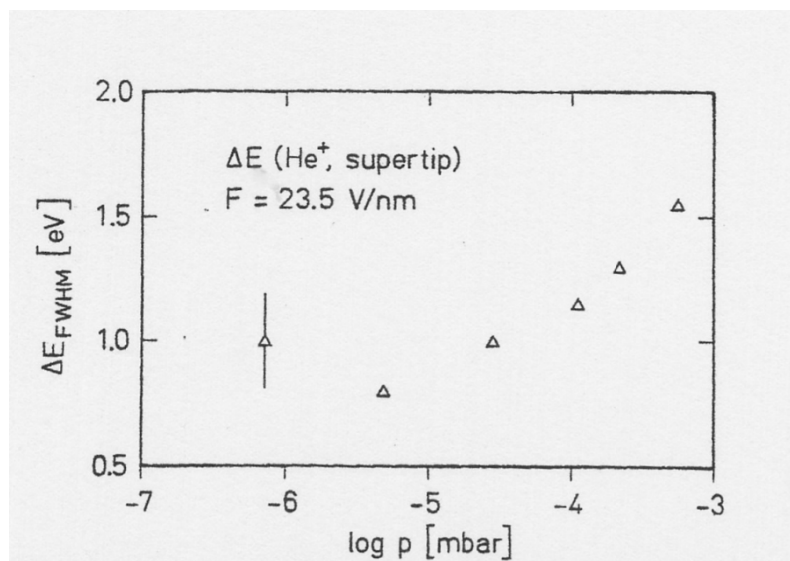


Figure 8. Two typical current-voltage characteristics at different gas temperatures

Figure 9. Emitter current vs. super-tip radius r_{sp} Figure 10. Energy spread of a super-tip He^+ beam as a function of gas pressure at a field of 23.5 V/nm

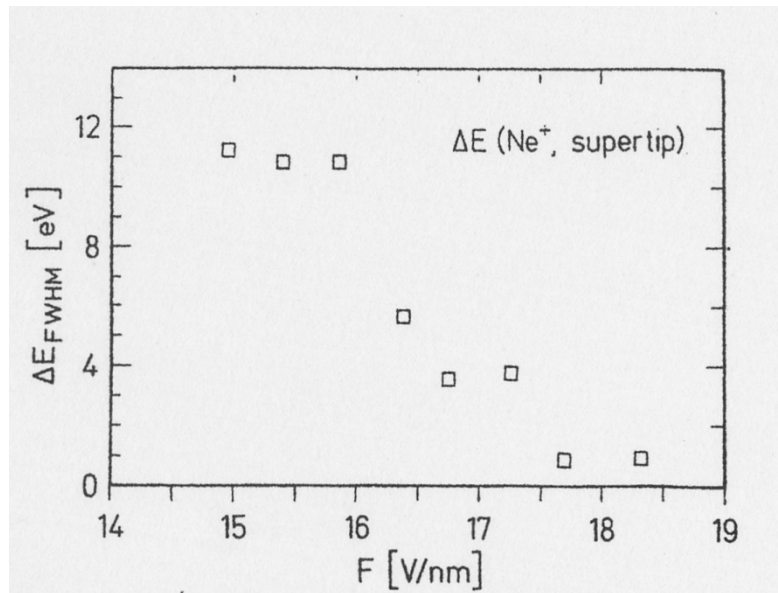


Figure 11. Energy spread ΔE of a super-tip Ne^+ beam as a function of field strength. Note the increase of ΔE at lower fields $F \leq 16 \text{ V/nm}$

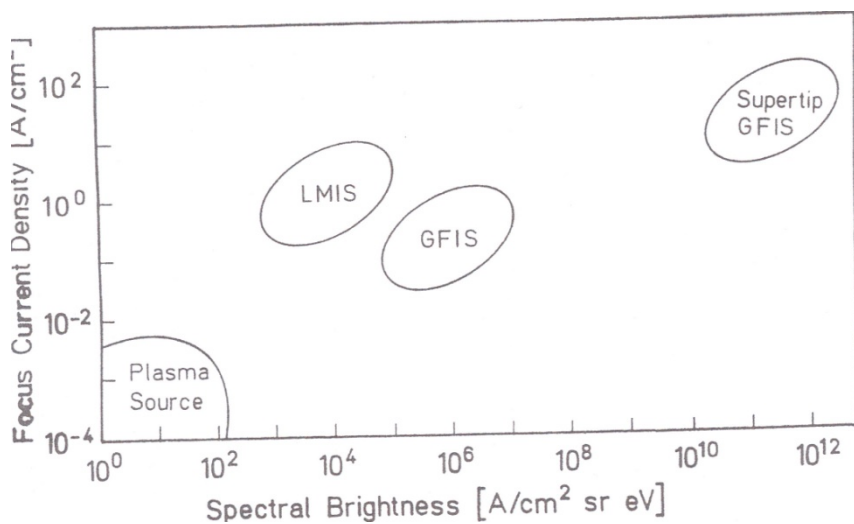


Figure 12. Comparison of different types of ion sources in terms of probe current and spectral brightness

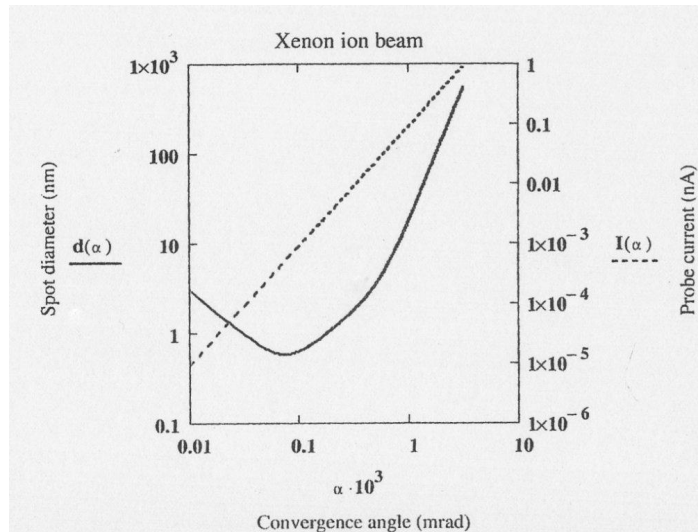


Figure 13. Image spot diameter $d(\alpha)$ and correlated probe current $I(\alpha)$ as a function of the convergence angle α . Source emitter current $I_s = 1$ nA. From right to left one sees three regimes of angular dependence: $d(\alpha) \sim \alpha^3$, $d(\alpha) \sim \alpha$, and $d(\alpha) \sim \alpha^{-1}$

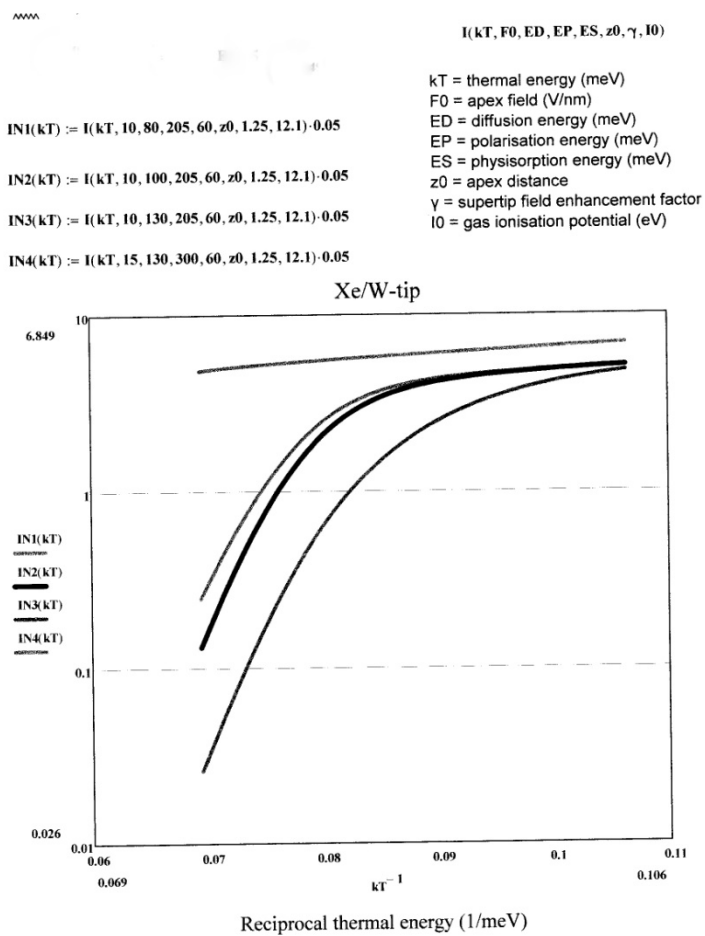


Figure 14. Calculated Xe^+ probe current $I(nA)$ for Xe diffusion energies of $Q = 80, 100$, and 130 meV. At the lower temperatures all curves are seen to merge to a common value of about $I \sim 5$ nA